geosciences

MDPI

Article

Tectono-Sedimentary Evolution of the Madrid Basin (Spain) during the Late Miocene: Data from Paleokarst Profiles in Diagenetically-Complex Continental Carbonates

Juan Carlos Cañaveras [1,*], Jose Pedro Calvo [2], Salvador Ordóñez [1], María Concepción Muñoz-Cervera [1] and Sergio Sánchez-Moral [3]

[1] Environmental and Earth Science Department, Faculty of Sciences, University of Alicante, Campus San Vicente del Raspeig, E-03690 Alicante, Spain; salvador@ua.es (S.O.); mc.munoz@ua.es (M.C.M.-C.)
[2] Mineralogy and Petrology Department, Faculty of Geological Sciences, Complutense University of Madrid, Ciudad Universitaria s/n, E-28040 Madrid, Spain; jpcalvo@geo.ucm.es
[3] Geology Department, MNCN-CSIC, C/José Gutiérrez Abascal, 2, E-28006 Madrid, Spain; ssmilk@mncn.csic.es
* Correspondence: jc.canaveras@ua.es

Received: 8 October 2020; Accepted: 29 October 2020; Published: 30 October 2020

Abstract: An intra-Vallesian (Upper Miocene) paleokarst developed at the top of the Intermediate Miocene Unit in the continental intracratonic Madrid Basin is recognized. This paleokarst is an early shallow, tabular-shaped karst that shows a marked control by the depositional facies pattern and lithologies. By integrating morphological, petrological, and geochemical data, three hydrogeological zones were established throughout the paleokarstic profiles: (i) a paleo-vadose zone, characterized by vertically elongated caves and vadose cementation; (ii) a 3–7 m thick paleo-epiphreatic zone (paleo-water table fringe), with development of stratiform breccia bodies, the superimposition of both vadose and phreatic features, and the lowest Fe and Mn contents in host-rock carbonates; and (iii) a paleo-phreatic zone characterized by an increase in $\delta^{13}C$ values and the predominance of phreatic cementation. The paleogeographic reconstruction for the intra-Vallesian paleokarst using profiles revealed relative topographic highs to the north and topographic lows to the south, drawing the paleokarst landscape. Immediately overlaying the paleokarst surface are fluvio-lacustrine facies belonging to the Miocene Upper Unit (Late Vallesian to Late Turolian). Their lowermost deposits consist of fluvial terrigenous facies deposited by approximately N–S fluvial streams, and pass upward into fluvio-lacustrine fresh-water limestones. This paleokarstic surface represents a major change in the evolution of sedimentary patterns of basin, from endorheic to exorheic conditions, as the result of a change from compressive to extensional conditions in the tectonic regime.

Keywords: paleokarst; dedolomite; meteoric diagenesis; stable isotopes; endorheic-exorheic transition; Miocene; Cenozoic Madrid Basin

1. Introduction

Subaerial exposure surfaces often limit and define stratigraphic units and sequence boundaries. The development and preservation of the features (e.g., rhizoliths, calcretes, diagenetic fabrics, paleokarst ...) that define those surfaces depends of several factors including duration of exposure, climate, sedimentary fabric and mineralogy, paleohydrology, paleotopography, and vegetation [1–5]. In the near-surface meteoric diagenetic environment, several hydrogeological or environmental zones (i.e., vadose and fresh-water phreatic zones) can be established. The interfaces between these zones are the main active diagenetic sites. In particular, the water table is considered to be a critical interface in diagenetic modeling because it is the boundary between the unsaturated vadose zone and the saturated phreatic zone. Both diagenetic processes and products are quite different in these zones,

so that the water table location controls the style and distribution of the chemical reactions throughout the diagenetic profiles. For this reason, the identification of paleo-water tables is a relevant tool in deciphering the depositional and diagenetic histories of a region and also in the paleogeographical and paleoenvironmental reconstruction of subaerial exposure surfaces. Karst researchers have often discussed the degree of applicability of the water table concept to karst systems because of the complexity of groundwater flows in this context [6] (see [7], pp. 64–69, for a concise and complete review). Some authors have transferred the water table concept unmodified to karst hydrology, but alternatively, other karst scientists have considered that independent conduit systems operate in a three-dimensional space. Despite this controversy, the need for differentiating vadose and phreatic features in regional-scale karst systems makes the use of the karst water table concept essential, especially in paleokarstic studies.

Water table positions have been inferred by petrographical and/or geochemical data in a large variety of Holocene [8–13], Pleistocene [14–19], and pre-Pleistocene settings [18,20–25]. However, in most of these examples, karstic features were scarce or absent. In modern and ancient examples of karst, the paleowater table position is inferred by geomorphological features as well as petrographic or geochemical data [1,26–28]. All of these studies show that diagenesis at subaerial exposure surfaces is highly variable, and hydrogeological or environmental zones and interfaces are dynamic. For this reason, their recognition and characterization in the rock record depend on a great variety of physical and chemical factors, and must be the result of a multidisciplinary study.

The present study focused on the determination of the position of the paleo-water table and the reconstruction of paleokarstic profiles in a Tertiary continental sequence. These materials were affected by early subaerial exposure which caused: (i) the formation of diagenetically-complex carbonates, and (ii) the development of paleokarstic features. The paper places emphasis on the integration of regional geologic, geomorphological, petrological, and geochemical data, derived from detailed analysis of the paleokarstic features and host-rock. A paleogeographic reconstruction of the Madrid Basin during the late Vallesian is inferred from this analysis.

2. Geological Setting

The Madrid Basin is an intracratonic basin located in the center of the Iberian Peninsula (SW Europe) (Figure 1A). The Neogene sedimentary infill of the basin reaches up to 800 m in thickness and includes three main Miocene units (Lower, Intermediate, and Upper Miocene Units) (Figure 1B). These units are mainly composed of lacustrine and alluvial deposits and are separated by major sedimentary discontinuities, which are represented by paleokarst and/or erosional surfaces. The materials we studied belong to the upper part of the Miocene Intermediate Unit. This unit is formed by a 50–200 m thick succession of continental sediments, ranging from Lower Aragonian to Late Vallesian (middle to upper Miocene) in age. The sediments display a concentric pattern of central chemical lacustrine facies, which grade laterally into progressively coarser-grained alluvial facies toward the basin margins. In the central and eastern part of the basin, the uppermost levels of the Miocene Intermediate Unit consist of shallow lacustrine deposits that are related to an episode of generalized lake expansion in the region [29]. These upper lacustrine beds show a large variety of diagenetic features that resulted from the transformation of dolostone, limestone, and gypsum, and were ultimately related to the karstification of the lake sequences (Figure 1C). An intra-Vallesian paleokarst outlines the sedimentary break between the Miocene Intermediate and Upper Units [30,31]. Immediately overlaying the paleokarst surface are fluvio-lacustrine siliciclastic/carbonate facies belonging to the Miocene Upper Unit. This Unit spans the Late Vallesian to Late Turolian and reaches up 50–60 m in thickness. Their lowermost deposits consist of fluvial terrigenous facies deposited by approximately N–S fluvial streams, and pass upward into fluvio-lacustrine fresh-water limestones, mainly deposited in the central and eastern basin. The facies arrangement shown by the fluvial deposits is clearly different from that observed in the earlier Miocene units, and suggests a major paleogeographical change in the area during the Vallesian, from endorheic to exorheic conditions [30,32]. The nature and distribution of

the Miocene Upper Unit was interpreted as the result of a change from compressive to extensional stress [33] partially opening the basin [31].

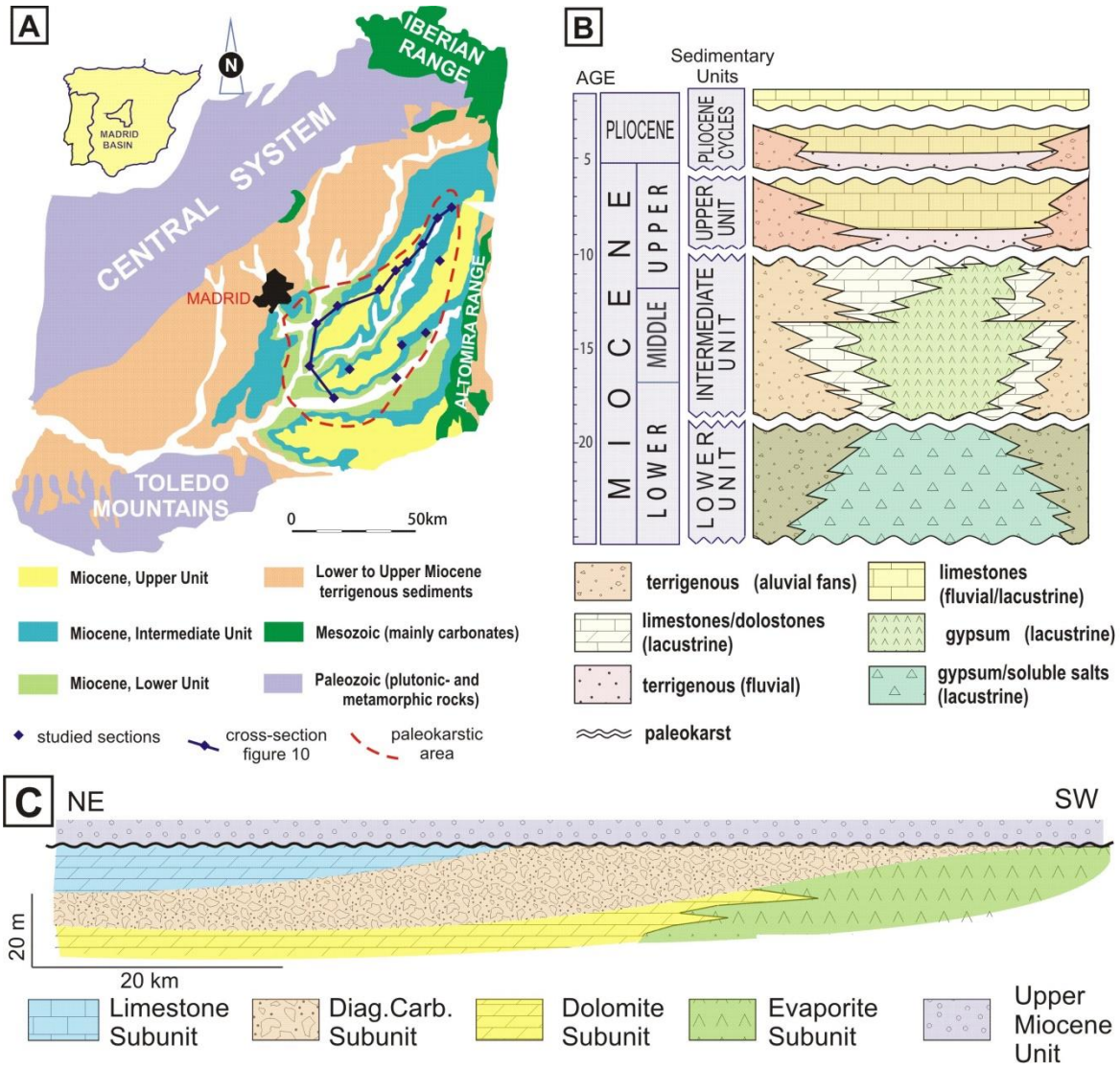

Figure 1. Geological features and lithostratigraphy of the Tertiary Madrid Basin. (**A**) Geographical and geological setting of the Madrid Basin with indication of the extension of the intra-Vallesian paleokarst (area encircled by the dashed line). (**B**) Stratigraphy of the Miocene sequence in the Madrid Basin. (**C**) Sketch of the spatial distribution of the main lithologies recognized at the top of the Miocene Intermediate Unit.

3. Materials and Methods

More than one hundred samples (host-rock, paleokarstic chemical, and detrital deposits) were collected for geochemical and petrographic study from 15 sections distributed along the entire study area (Figure 1A). Petrographic conclusions are based on the examination of standard and double-polished thin sections by conventional transmitted light microscopy. Etched and unetched specimens of rock fragments and polished thin-sections were studied using two microscopes: (i) the FEI QUANTA 200 apparatus of the Museo Nacional de Ciencias Naturales (MNCN-CSIC) laboratories working at 30 kV; and (ii) a JEOL JSM-6400 at the ICTS-CNME Complutense University of Madrid (Universidad Complutense de Madrid, Spain) working at 20 kV. X-ray diffraction was used to determine mineral composition in powdered carbonate samples and insoluble residues using quartz

as an internal standard. Mole percent magnesium carbonate in calcite was estimated by measuring the d_{104} spacing. The analyses were performed by using a PHILIPS PW-1710 XR-diffractometer (Amsterdam, Netherlands, MNCN-CSIC) operating at 40 kV and 30 mA, under monochromatic CuKα radiation. Major and trace element contents (Ca, Mg, Sr, Fe, Mn, and Na) from 142 samples were determined by x-ray fluorescence (PHILIPS 1410/20 XRF spectrometer, Amsterdam, Netherlands, MNCN-CSIC) using standard techniques. Oxygen and carbon isotope values from 41 selected samples were determined at the GEOTOP Laboratory (Canada) using standard procedures and the results are given in the delta-notation as the permil (‰) deviation relative to the Vienna Pee Dee Belemnite (VPDB) standard.

4. Results and Discussion

4.1. Petrology of the Top of the Miocene Intermediate Unit

Four different lithological subunits mainly composed of dolostones, limestones, gypsum, and diagenetically-complex micro-pseudosparites (herein termed 'diagenetic carbonates') can be distinguished at the upper part of the Miocene Intermediate Unit (Figure 1C):

- Dolomite Subunit—This subunit comprises decimeter-thick beds of dolomicrites, dolomitic marlstones, micrites, and claystones. The dolomicrites contain abundant lenticular gypsum traces that occur as either preserved within the dolostones or as calcite pseudomorphs. Desiccation and pedogenic traces such as shrinkage cracks, root casts, and brecciation are locally present. Fossil remains are scarce and consist mainly of charophyte gyrogonites and ostracod shells. XRD analyses indicate that dolomicrite beds are mainly composed of dolomite or dolomite–calcite mixtures. The dolomites showed quite variable mole %$MgCO_3$ contents, ranging from 46 to 49%, whereas the calcites showed mole % $MgCO_3$ contents lower than 3.
- Evaporite Subunit—This subunit comprises decimeter-thick gypsum beds with cm-thick intercalations of clays and marls. Gypsum consists mainly of meso and macrolenticular fabrics, many of them showing a bimodal size-distribution of the gypsum lenses. Burrowing features and chert nodules are common in this facies.
- Limestone Subunit—This subunit consists of decimeter to meter-thick tabular limestone beds with thin clay intercalations. The limestones include mudstones and peloidal-intraclastic wackestones with abundant pedogenic features (root traces, bioturbation, desiccation cracks). Evidence of lacustrine biota (charophytes, ostracods, and gastropods) and disperse lenticular molds or pseudomorphs are also common in these fabrics. XRD analyses indicate that limestones are mainly composed of low magnesian calcite, ranging from 0 to 3 mole % $MgCO_3$.
- Diagenetic Carbonate Subunit—This is a complex subunit comprising diagenetic carbonate beds that overall forms a stratiform zone. The contact with the underlying dolomicrite and gypsum deposits is locally sharp and irregular, whereas it is seen to be transitional in other places. The diagenetic carbonates occur either as well-defined beds or irregular-shaped bodies comprising coarse chaotic breccias. To the south, where underlying gypsum beds are predominant, the diagenetic zone is narrow, discontinuous, and internally brecciated, showing abundant fragments of speleothems. A great variety of diagenetic carbonate fabrics are found within this subunit. Most of them have been interpreted as paleo-groundwater alteration products after shallow-lacustrine dolomicritic deposits [34,35], although neomorphic and replacive fabrics after gypsum are also present. Petrographically, the dedolomites show a great variety of fabrics, which occur in many places mixed within the same bed. They are composed of meso-macrocrystalline xenotopic mosaics of inclusion-rich (mainly composed of Fe-oxides and fibrous clays) calcite crystals. The crystal shapes are quite variable including: (i) sutured crystals with serrated or irregular intercrystalline boundaries (Figure 2A); (ii) spheroidal crystals displaying an internal radial-fibrous microstructure ('pesudospherulitic fibrous calcites') (Figures 2B and 3A); and (iii) rhombic to subrhombic zoned crystals (Figure 2C). All these

crystals are predominantly non-luminescent under CL, occasionally with thin dull and brightly orange luminescent laminae. Some crystal cores may contain microdolomite inclusions (Figure 3B). Lenticular gypsum pseudomorphs and ghosts are disseminated throughout the mosaics (Figure 2D). The intercrystalline matrix is formed mainly of fibrous magnesian clays (sepiolite and palygorskite) (Figure 3C) with a minor proportion of microspar, Fe-oxides, and terrigenous grains. Calcitization after gypsum fabrics resulted in: (i) xenotopic mesocrystalline mosaics with abundant lenticular pseudomorphs and bioturbation structures; (ii) microcrystalline mosaics with relicts of gypsum; and (iii) micro-mesocrystalline mosaics with clotted or grumelose texture. The latter grades into either lenticular primary gypsums or other calcitization fabrics at the outcrop scale. All diagenetic carbonate fabrics are mainly composed of low magnesian calcite, ranging from 0 to 3 mole % $MgCO_3$; only some samples contained small proportions of dolomite (<4%).

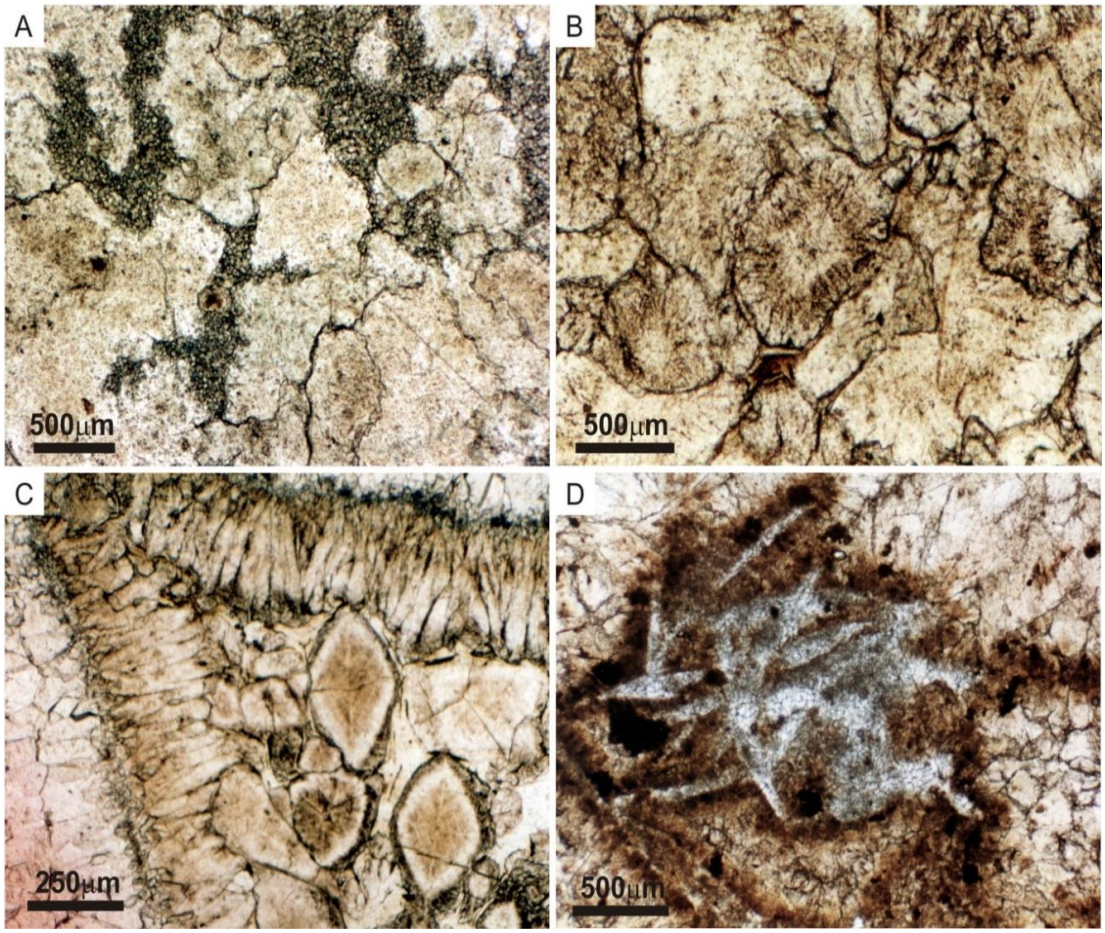

Figure 2. Thin section photomicrographs showing dedolomite fabrics in the Diagenetic Carbonate Subunit. (**A**) Sutured mosaic composed of inclusion-rich anhedral crystals. (**B**) Xenotopic mosaic including pseudospherulitic fibrous calcite crystals. (**C**) Rhombic and subrhombic zoned crystals forming a xenotopic mosaic between macrolenticular pseudomorphs. (**D**) Detail of lenticular pseudomorph aggregate. All photomicrographs were taken under plane-polarized light.

As discussed in [34], gypsum dissolution has been pointed out as the driving mechanism for diagenetic alteration processes, especially in dedolomites. The calcitization of both dolostone and gypsum occurred at shallow burial depths within the diagenetic phreatic environment, and was achieved by the action of meteoric-derived water. Calcitization processes took place early after the deposition of the top of the Miocene Intermediate Unit and were closely related to karstification.

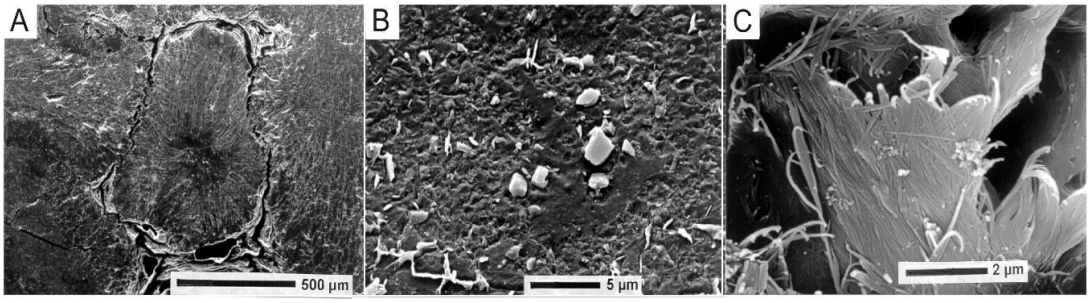

Figure 3. Scanning-electron micrographs corresponding to pseudospherulitic fibrous calcite mosaics. (**A**) General view of a pseudospherulite crystal. Intercrystalline matrix is mainly formed by fibrous magnesian clays. (**B**) Detail of microdolomite inclusions in the core of a pseudospherulite crystal. (**C**) Intercrystalline matrix: detail of a mat of interwoven sepiolite fibers.

4.2. Geochemistry

Data obtained by trace-element and stable isotope analyses are summarized in Table 1. Mg contents from carbonates belonging to the Dolomite Subunit were higher than those determined in the overlying diagenetic carbonates and limestones. Mg contents of speleothems were similar to their host-rock (diagenetic carbonates and limestones), ranging from 0.5 to 2.5% (Table 1). Despite the fact that Na has been questioned as a salinity marker by several authors [36,37], we interpreted the low Na contents of the analyzed samples as related to low salinity conditions [38,39]. Our interpretation is consistent with regional geological evidence that dilute, freshwater conditions prevailed during the deposition of the uppermost part of the Miocene Intermediate Unit [30,40], and the sustained evidence of freshwater diagenesis affecting the Miocene lacustrine deposits. The low Fe and Mn contents of the diagenetic carbonates and speleothems are indicative of oxidizing conditions and/or the absence of a source for Fe and Mn other than preexisting carbonates [41–43].

Table 1. Summary of the geochemical composition of carbonates from the paleokarstic profiles. See Figure 1C for spatial distribution of the lithological subunits. Values are expressed in %, except for Mn and Sr (ppm). n: number of samples; µ: mean values; σ: standard deviation.

	Dolomite Sub.			**Diag. Carb. Sub.**			**Limestone Sub.**			**Speleothems**		
	n	**µ**	**σ**	**n**	**µ**	**σ**	**n**	**µ**	**σ**	**n**	**µ**	**σ**
Ca	16	25.70	6.06	64	37.4	2.11	36	38.8	0.95	26	38.24	1.14
Mg	16	8.96	4.16	64	0.46	0.30	36	0.32	0.24	26	0.56	0.49
Na	16	0.06	0.04	64	0.08	0.14	36	0.08	0.16	26	0.06	0.11
Sr	16	414	362	64	215	249	36	250	149	26	81	51
Fe	16	0.42	0.53	64	0.24	0.24	36	0.20	0.28	26	0.13	0.12
Mn	16	189	113	64	50	18	36	66	50	26	37	22
$\delta^{18}O$	1	−0.33		19	−6.48	0.23	5	−6.50	0.10	16	−6.72	0.42
$\delta^{13}C$	1	−6.15		19	−8.27	0.70	5	−8.66	0.35	16	−9.2	0.73

The low ^{18}O contents in all samples could be interpreted as indicative of the influence of meteoric waters with low $\delta^{18}O$ values [44]. The dolomicrite samples [40,45] show a wide range (−8 to 0‰) of $\delta^{18}O$ values, indicating moderately evaporitic to relative fresher conditions, the latter being specially marked in samples with abundant pedogenic features. The role of plants in forming the carbonates is indicated by the relatively low $\delta^{13}C$ values, reaching up to −10‰ [40]. The low $\delta^{13}C$ values of the diagenetic carbonates may be explained by the contribution of carbon from the relatively ^{12}C-enriched parent material and, to a some extent, from ^{12}C-enriched soil-derived CO_2 [5,46–49]. The lower $\delta^{13}C$ values of speleothems could be indicative of the weak influence of the host-rock composition in the genesis of the speleothems. This fact could reflect either that the water–rock ratio is low, or diagenetic stabilization has been reached, or both.

4.3. The Intra-Vallesian Paleokarst

Paleokarst features such as caves, collapse breccias, or speleothems extend 10–35 m downward from the intra-Vallesian paleokarstic surface into the uppermost levels of the Miocene Intermediate Unit. This surface displays morphologies indicative of erosion (e.g., paleochannels) and solution-collapse phenomena, which resulted in a maximum preserved topographic relief of about 15 m.

4.3.1. Exokarstic Features

Two main types of morphological features are present on the top of the Miocene Intermediate Unit: small bowl-shaped depressions (dolines) and gently sloping fluvio-karstic valleys. Dolines range from 0.5 to 5 m in depth and 5 to 20 m in diameter. At outcrop, the maximum topographic depth of fluvio-karstic valleys is about 5 m. Both types of exokarstic morphologies are interpreted as resulting from surficial dissolution and gravitational collapses due to the erosion and dissolution of near-surface caves and, in the case of the valleys, also by stream (fluvial) erosion.

The exokarstic infill-facies consist of chaotic carbonate breccias and siliciclastic deposits of the overlying sequences (Miocene Upper Unit) (Figure 4). The breccias are poorly sorted and clast-supported with a marly, occasionally sandy, matrix. The clasts range 5 cm to more than 1 m in size, and are derived from the erosion and/or collapse of host-rock and from karst-generated deposits (speleothems and internal sediments). They are formed by the removal of the underlying carbonates and subsequent foundering of the cave walls and roof at the shallow levels of paleo-endokarstic galleries. Laminated and/or nodular marly to carbonate deposits are also locally present in paleo-exokarstic depressions (Figure 4).

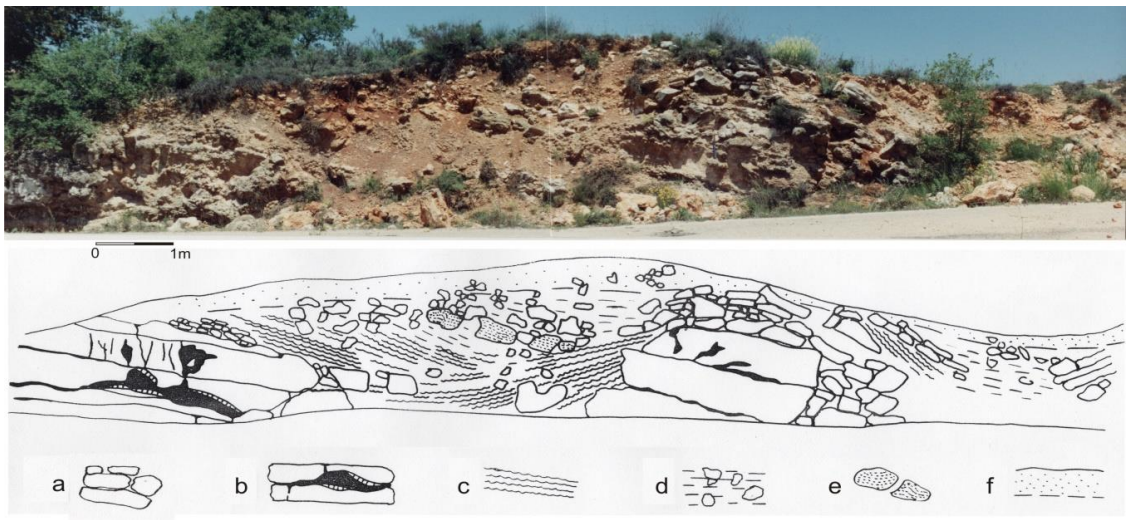

Figure 4. Detail of some paleo-exokarstic features affecting the top of the Miocene Intermediate Unit in the northern part of the basin. (**a**) Micritic limestones (Limestone Subunit) in breccioid and tabular beds. (**b**) Cavities with fine-grained siliciclastic infills and fibrous speleothems. (**c**) Nodular lutite beds. (**d**) Lutite massive levels with dispersed limestone gravels. (**e**) Decimeter-thick fragments of nodular to laminated limestone beds (fragments of paleosoils and/or doline sedimentary infills). (**f**) Modern soil.

The siliciclastic fills usually comprise clays and sandstones, although gravels are locally abundant. The clay mineralogy is dominated by illite and smectite, whereas the composition of the sandstones is mainly subarkosic. This composition is consistent with those of the border siliciclastic facies of the Intermediate Unit and lowermost deposits of the Upper Unit [30,32]. The clay and sand fraction of the breccia matrix showed a similar mineralogy. The onlap relationship between the siliciclastic deposits and the carbonate substrate clearly indicates that their formation was conditioned by the presence of an earlier paleokarstic relief.

4.3.2. Endokarstic Features

- Caves—The endokarstic arrangement of the paleokarst is mainly characterized by a poorly preserved network of horizontally elongated caves vertically connected by oblique irregular conduits. Some vertically elongated caves can be recognized in the uppermost levels of both the Limestone and Diagenetic Carbonate Subunits. This morphological pattern is thought to have been mainly developed by dissolutional processes affecting the soluble rocks (e.g., gypsum beds) and strata discontinuities (bedding planes and joints) in a shallow phreatic environment [31]. Constraints imposed by the present outcrop topography and by later (Quaternary) karst overprints make precise geometric determinations of these paleocaves difficult. Caves are partially to completely filled by a combination of collapse breccias, siliciclastic infill deposits, and speleothems (Figure 5).

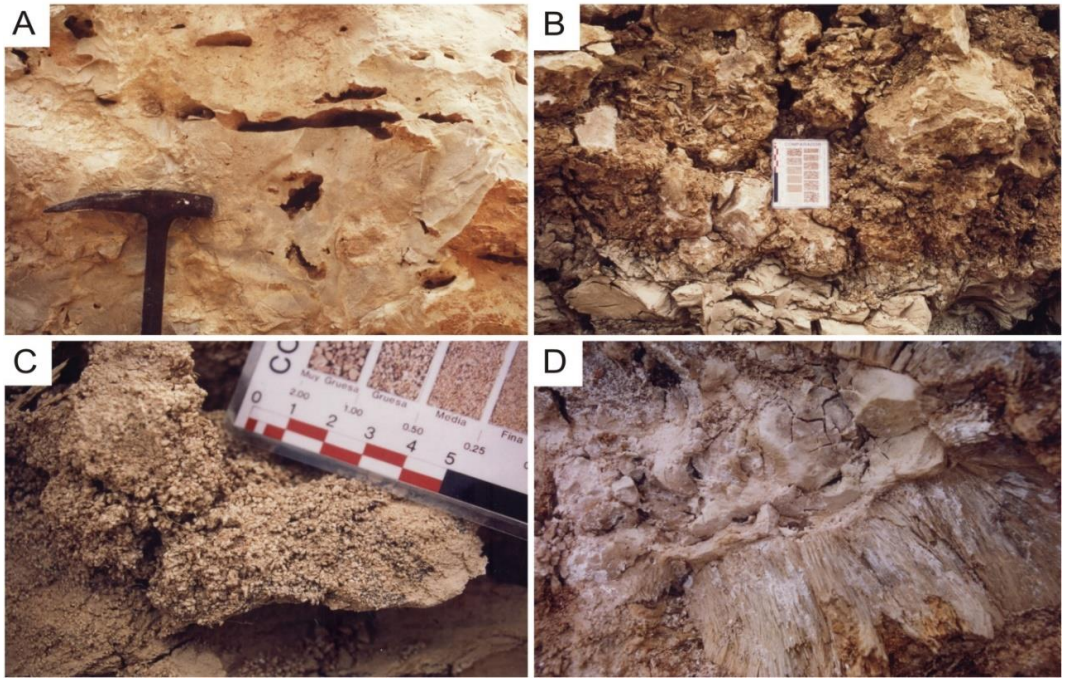

Figure 5. Paleokarstic features. (**A**) View of predominantly horizontal caves and vugs below the upper limit of the water table fringe in (paleokarstic profile of type I). (**B**) Detail of clast-supported collapse breccia (paleokarstic profile of type I). Clasts are mainly composed of pseudospar fragments with abundant calcite pseudomorphs after lenticular gypsum crystals (arrows). (**C**) Macrocrystalline sand deposit associated to breccia bodies (paleokarstic profile of type I). (**D**) Detail of a 10 cm-thick coarse fibrous speleothem growing on micritic limestone (paleokarstic profile of type I).

- Vugs—Small caves and passageways, herein termed vugs, are common and occur throughout all subunits. Vugs have irregular walls and a maximum dimension ranging from 1 to 15 cm (Figure 5A). They display a preferred orientation with depth, being predominantly horizontal at greater depths. There are high concentrations of vugs with the obliteration of bedding in some areas, preferentially close to collapse breccia bodies. These areas of high vuggy porosity suggest intense leaching of rock by groundwater [50]. Horizontally oriented vugs are usually rimmed by isopachous bladed calcite cements. In vertically oriented vugs, the sediments are rare, and consist commonly of discontinuous bladed to micrite calcite cements.
- Collapse breccias—Collapse breccia bodies are very variable in thickness and lateral extent. Most of them are parallel to the bedding. Two types of breccia bodies can be recognized: (i) Tabular to podlike bodies (3–20 m long, and 0.5–5 m wide), and (ii) larger stratiform bodies (5–30 m wide, and some hundreds of meters long). Breccias are clast-supported (Figure 5B) with a clayey to sandy matrix, which is more abundant in the tabular breccia bodies. The mineral composition of

the clay fraction is similar to those of the exokarstic breccias. However, the sandy matrix mainly consists of rhombic to pseusdospherulitic calcite crystals; in some sections, these sandy crystals form discontinuous accumulations up to 5 cm-thick (Figure 5C). Clasts consist of fragments of pseudospar, limestone, and minor speleothems. The origin of smaller breccia bodies is related to internal gravitational collapses and crumbling of the caves, the process being triggered by dissolution and subsequent mechanical instability of cave walls and roofs. The origin of larger breccias bodies is related to internal gravitational collapses of the caves and/or gradual brecciation due to evaporite dissolution. Matrix in cave sediments represents infiltration of soil into caves or accumulation of insoluble residue resulting from dissolution of host-rock. The sandy matrix is clearly related to partial dissolution and disaggregation of clay-rich pseudosparitic host-rock. The abundance and areal continuity of collapse breccia in the Diagenetic Carbonate Unit suggests that this unit was a significant paleohydrologic conduit during paleokarstification stages.

- Siliciclastic infills—The siliciclastic infill deposits consist of 20–60 cm thick tabular sandstone beds that can be followed laterally from 2 to 5 m (Figure 6). The sandstone beds occur commonly intercalated with thin layers of lutites and clays in the cave interiors. These deposits are petrographically equivalent to the exokarstic infill sandstones, thus suggesting: (i) they were also sourced by the clastic deposits of the Miocene Upper Unit that covers the karst surface, and (ii) karstification was active during the first stages of Upper Unit deposition.

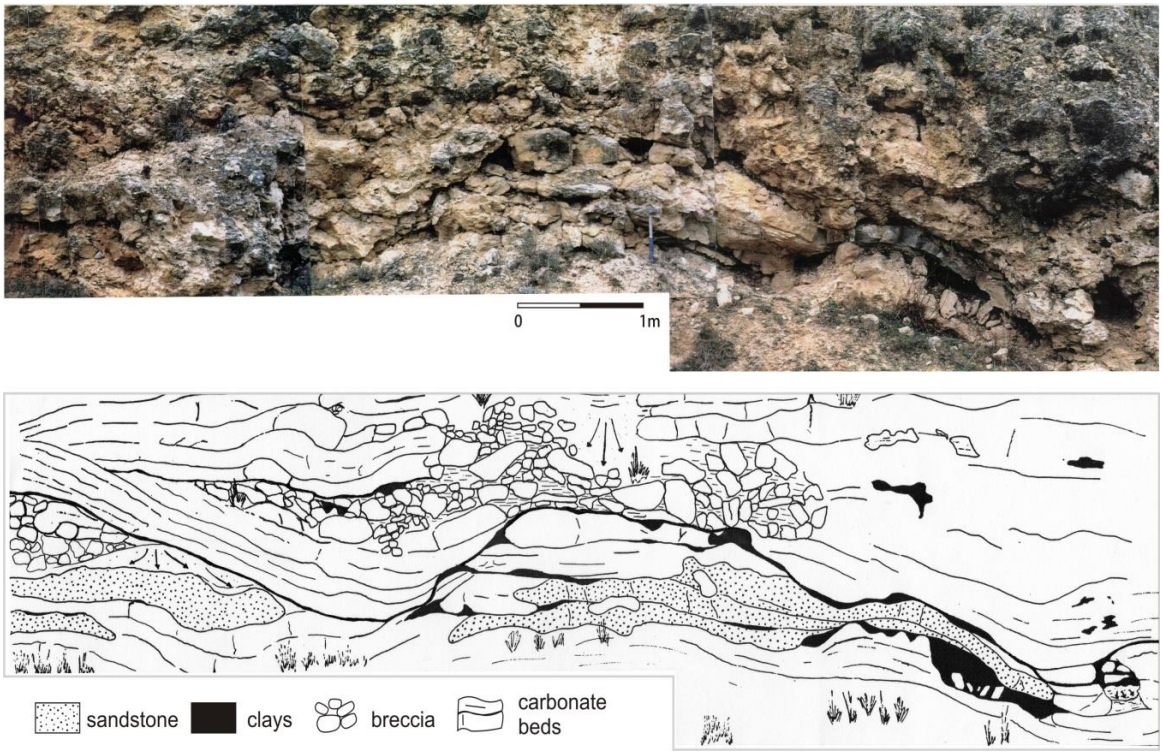

Figure 6. Detail of some paleokarstic features affecting the top of the Miocene Intermediate Unit in the central part of the basin. Note the original geometry of 'paleo' caves displayed by the lateral extent and thickness of the terrigenous infill deposits, which consist of arkosic sandstones (dotted) and clays (black). Irregular-shaped bodies of karstic carbonate breccias are also present.

- Speleothems—Speleothems form more or less continuous crusts on the cave floors, walls, and ceilings, and are also found as fragments in endo- and exokarstic breccias (Figure 5D). In thin section, these precipitates consist of anastomosing bundles of fibrous and columnar calcite crystals with rhomb terminations (Figure 7A,B). Their thicknesses range from 0.5 to 40 cm. Discontinuous banded speleothems (flowstones) associated with siliciclastic cave infills are

recognized in the uppermost levels of the sequences. Continuous coarse fibrous speleothems are usually related to underlying levels where stratiform breccia bodies are abundant. Spar cements composed of clear, iron-poor, blocky calcite crystals with dog-teeth terminations are also present (Figure 7A). These cements form isopachous coatings on the breccia clasts or are lining fissures or vugs. Both speleothems and spar cements are nonluminescent, occasionally with thin bright bands, suggesting formation from oxidizing meteoric groundwater at shallow depths. Pendant bladed- and micrite cements (Figure 7C,D) and vadose silts (Figure 7B) are also present along the paleokarstic profiles. These features are interpreted as vadose in origin.

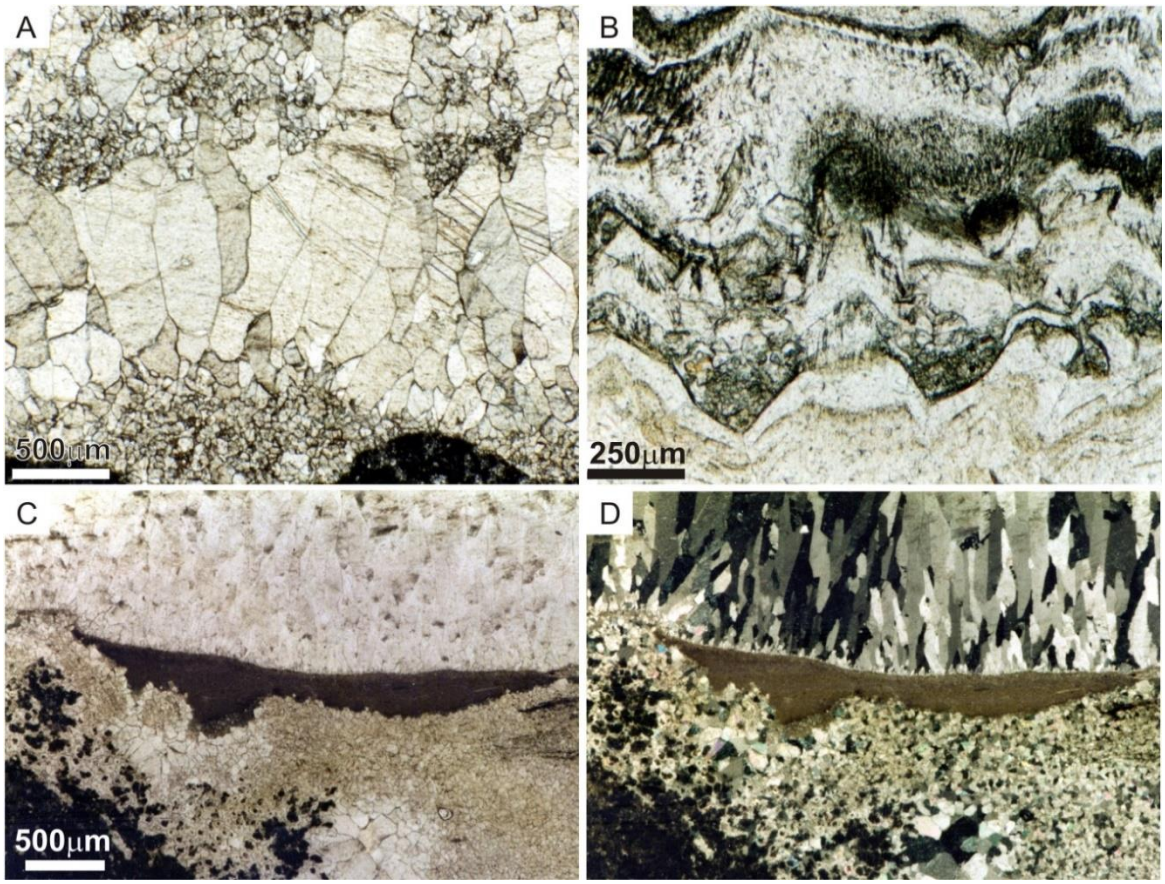

Figure 7. Thin section photomicrographs showing vadose and phreatic features affecting the top of the Miocene Intermediate Unit. (**A**) Isopachous void-filling spar cements; note two generations of dogtooth cements (phreatic zone) separated by vadose silt. (**B**) Detail of vadose silt at the top of a 'paleo'-flowstone speleothem. (**C**,**D**) Micrite (vadose) cement partially lining a solution cavity, followed by the generation of dogtooth spar cement (phreatic zone). All photomicrographs were taken under plane-polarized light except (**D**), which was taken under crossed nicols.

4.3.3. Paleokarst Profiles

The types and extent of karst features we have recognized vary along the length of the study area. This reflects a rather complex history of dissolution and further collapse/infilling processes developed on calcareous and gypsiferous continental sediments during a subaerial exposure interval. As in other meteoric settings, at least two hydrogeological zones can be established in karsttified aquifers: the vadose and the phreatic zones, the two zones being separated by the water table interface or epiphreatic zone. The water table is a dynamic interface strongly affected by short-term oscillations, so the water table interface can be thought of as including the overlying capillary fringe and the uppermost part of the phreatic zone [7]. Several geomorphological and petrographic features are

diagnostic for detecting and/or predicting the position of the paleo-water table [8–10,14,17,51–54]: (i) the geometry and distribution of the preserved caves; (ii) the distribution of collapse breccia and clastic infill sediments; and (iii) the types and distribution (vadose vs. phreatic) of meteoric cements and speleothems.

Four types of paleokarst profiles have been differentiated, attending to the distribution of karstic features and the nature of host-rock. These paleokarst profiles characterize distinct areas in the basin (Figure 8):

- Type I—This profile represents the NE part of the study area. Therein, the paleokarstic features were developed on diagenetic carbonates and limestones. The profile thickness ranged from 12 to 20 m. A 3–5 m thick water-table fringe was established in this profile. This fringe is characterized by the development of extensive endokarstic brecciation, the existence of abundant speleothems, and the juxtaposition of vadose and phreatic cement types. Speleothems in this fringe display continuous coatings on both caves walls and breccia fragments. The most distinctive features characterizing the vadose zone are: (i) irregular depressions that are usually filled by terrigenous facies with intercalations of pedogenic levels and/or mantling carbonate breccias; (ii) vertically elongated caves and vugs; (iii) discontinuous speleothems; and (iv) vadose (gravitational) cements. Alternatively, the paleo-phreatic zone is characterized by clast-supported breccia forming tabular to irregular bodies, and rare continuous fibrous speleothems.
- Type II—Mainly present in the central part of the basin, this type of profile was developed on diagenetic carbonates and extended 10–30 m downward. As in type I, the arrangement of exokarstic features is indicative of a low relief paleolandscape. The profiles are formed of a thick breccia zone, where abundant endokarstic features including speleothems, siliciclastic infills (lutites and sandstones), and tabular to irregular collapse-breccias can be recognized (Figure 7). The location of the water table cannot be accurately fixed, because this type of profile is characterized by wide and heterogeneous distribution of endokarstic features. This could be indicative of a high range of fluctuation and/or the existence of a great number of gypsum intercalations.
- Type III—This was present at the eastern part of the basin. The paleokarstic profiles were mainly developed on limestones and are characterized by a large occurrence of exokarstic features. These features include dolines and other karstic depressions, which give place to the formation of a paleorelief with marked differences (10–20 m) in topography. The exokarstic sediments consist of carbonate breccia and siliciclastic infills, the latter being composed of lutites and sandy lutites with intercalations of sandstones and carbonates (paleosols and oncolites). Endokarstic features such as speleothems and breccia are rare and their discrimination from exokarstic features places some uncertainty. This seems to indicate that vadose conditions prevailed during the formation of this type of profile, though the precise position of paleowater table cannot be fixed.
- Type IV—This type of paleokarstic profile was mainly developed on gypsum deposits that crop out in the southern part of the basin. As aforementioned, this profile consists of a narrow and irregular carbonate breccia stratiform zone. Clasts are formed of fragments of fibrous speleothems and diagenetic carbonates that resulted from gypsum calcitization. These carbonates may be considered as a 'residual' deposit after extensive gypsum dissolution.

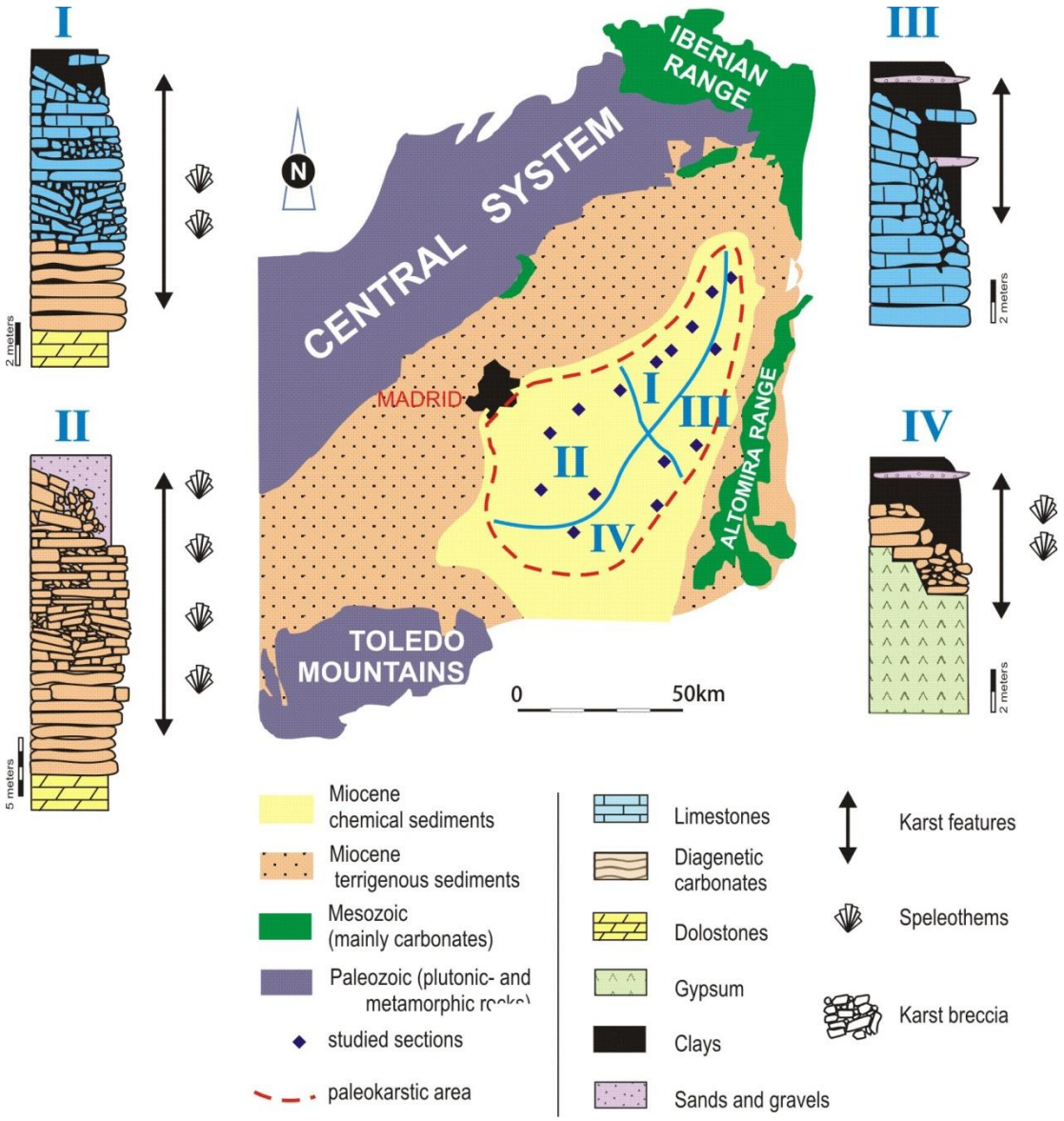

Figure 8. Main types of paleokarstic profiles and their spatial distribution across the study area (check Figure 1C for integration of the lithostratigraphic background). Roman numbers indicate the different paleokarstic areas distinguished. See text for explanation.

In summary, the morphological, sedimentological, and petrographic features of the paleokarst allow precise definition of the environmental and hydrogeological zonation for the profiles of type I. In the other profile types, these features are not diagnostic enough to clearly display the location of the paleowater table within the paleokarstic sections. In order to establish a general model for the geochemical evolution of the paleokarst that could be extrapolated to the other profiles throughout the basin, the profiles of type I were selected to carry out a thorough geochemical (trace element and stable isotopes) characterization of the paleokarst materials.

The geochemical characterization of the different environmental zones for the paleokarstic profiles are given in Table 2 and in Figure 9. The water table fringe in the paleokarstic profiles of type I is characterized by carbonates showing the lowest Mg, Fe, and Mn contents and by an increase in $\delta^{13}C$ below this zone. Below the water table fringe, host-rock was 0.4–1.5‰ enriched in ^{13}C relative to the uppermost carbonates. In the central part of the study area, represented by paleokarstic profiles of type II, the distribution of trace elements and isotope signatures was quite similar to that obtained in the northeastern area. The carbonates coincident with the water table fringe were also characterized

by the lowest Mg, Fe, and Mn contents, though the thickness of the fringe was markedly higher (approximately twice).

Table 2. Summary of the trace element and stable isotopic composition of the hydrogeological zones that constitutes the three main types of paleokarstic profiles of the intra-Vallesian paleokarst. All values are expressed in %, except for Mn and Sr (ppm). n: number of samples; μ: mean values; σ: standard deviation; H: host-rock (limestone, dolomicrite, diagenetic carbonate); S: speleothems.

			Mg			Na		Sr		Mn		Fe		$\delta^{18}O$			$\delta^{13}C$	
			n	μ	σ	μ	σ	μ	σ	μ	σ	μ	σ	n	μ	σ	μ	σ
Profile type I	vadose	**H**	19	0.39	0.30	0.13	0.19	148	133	71	51	0.25	0.13	7	−6.60	0.22	−8.60	0.40
		S	7	0.27	0.23	0.12	0.15	37	31	45	14	0.13	0.10	3	−6.50	0.50	−8.50	1.05
	water-table	**H**	8	0.27	0.11	0.03	0.06	279	264	36	4	0.09	0.05	2	−6.50	0.01	−9.00	0.10
		S	2	0.25	0.06	<0.01	-	72	62	45	7	0.06	0.03	2	−6.55	0.16	−9.30	0.03
	phreatic	**H**	33	1.60	3.02	0.09	0.14	234	276	61	24	0.36	0.28	6	−6.30	0.18	−8.05	0.52
Profile type II	vadose	**H**	7	0.32	0.20	0.02	0.03	513	571	51	15	0.16	0.15	1	−6.95	-	−9.10	-
		S	4	1.10	1.00	0.01	0.01	110	40	22	15	0.14	0.17	2	−6.35	0.69	−8.60	0.60
	water-table	**H**	11	0.35	0.33	0.13	0.14	164	126	35	7	0.06	0.05	2	−6.50	0.10	−8.90	0.00
		S	8	0.64	0.37	0.05	0.11	339	445	46	30	0.19	0.15	5	−7.00	0.25	−9.70	0.30
	phreatic	**H**	14	7.70	5.00	0.01	0.02	294	188	132	53	0.42	0.58	3	−6.40	0.08	−8.00	0.20
Profile type III	vadose	**H**	7	0.17	0.15	0.02	0.03	294	186	69	66	0.14	0.09	-	-	-	-	-
		S	1	0.30		<0.01	-	87	-	31	-	0.15	-	-	-	-	-	-
	water-table	**H**	5	0.22	0.15	0.19	0.16	400	144	58	34	0.07	0.04	1	−6.50	-	−8.89	-
		S	-	-	-	-	-	-	-	-	-	-	-	4	−6.70	0.19	−9.40	0.39
	phreatic	**H**	12	0.18	0.15	0.02	0.05	256	100	57	32	0.27	0.45	2	−6.50	0.23	−7.00	0.98
		S	4	0.42	0.03	0.08	0.12	85	17	26	1	0.06	0.02	-	-	-	-	-

As in the northeastern area, speleothems belonging to the uppermost levels of the Miocene Intermediate Unit were also enriched in ^{18}O and ^{13}C. In the eastern part of the study area (paleokarstic profiles of type III), the geochemical zonation was less resolute and reliable when compared with the results obtained in the northeastern and central areas. Within these profiles, the distribution of trace elements did not show a clear vertical trend from which geochemical zonation could be deduced. Nevertheless, the water table fringe, approximately 3 m thick, would also be characterized geochemically by low Fe contents as well as by heavier ^{13}C contents of the carbonate below this zone. The distribution of trace element and isotopic values in sections of the southern part of the study area, represented by paleokarstic profiles of type IV, has not been analyzed since the carbonates in these sections are mainly regoliths formed after extensive gypsum dissolution. This fact prohibits obtaining good resolution of the geochemical trend through the profiles.

The Mg contents of speleothems usually show an erratic trend throughout the profiles (Figure 9) due to the interplay of several factors: (i) during the precipitation of speleothem carbonate, evaporation and degassing drive up fluid saturations [55]; (ii) alternatively, some speleothems formed in the water table fringe, an open water-dominated diagenetic subenvironment in which the chemistry of the circulating water is mostly controlled by host-rock dissolution rates; and (iii) the processes of speleothem growth and dedolomitization are closely related during the early karstification of the Miocene carbonates, resulting in the high availability of magnesium, which may support the erratic trend observed in the Mg contents of the speleothems.

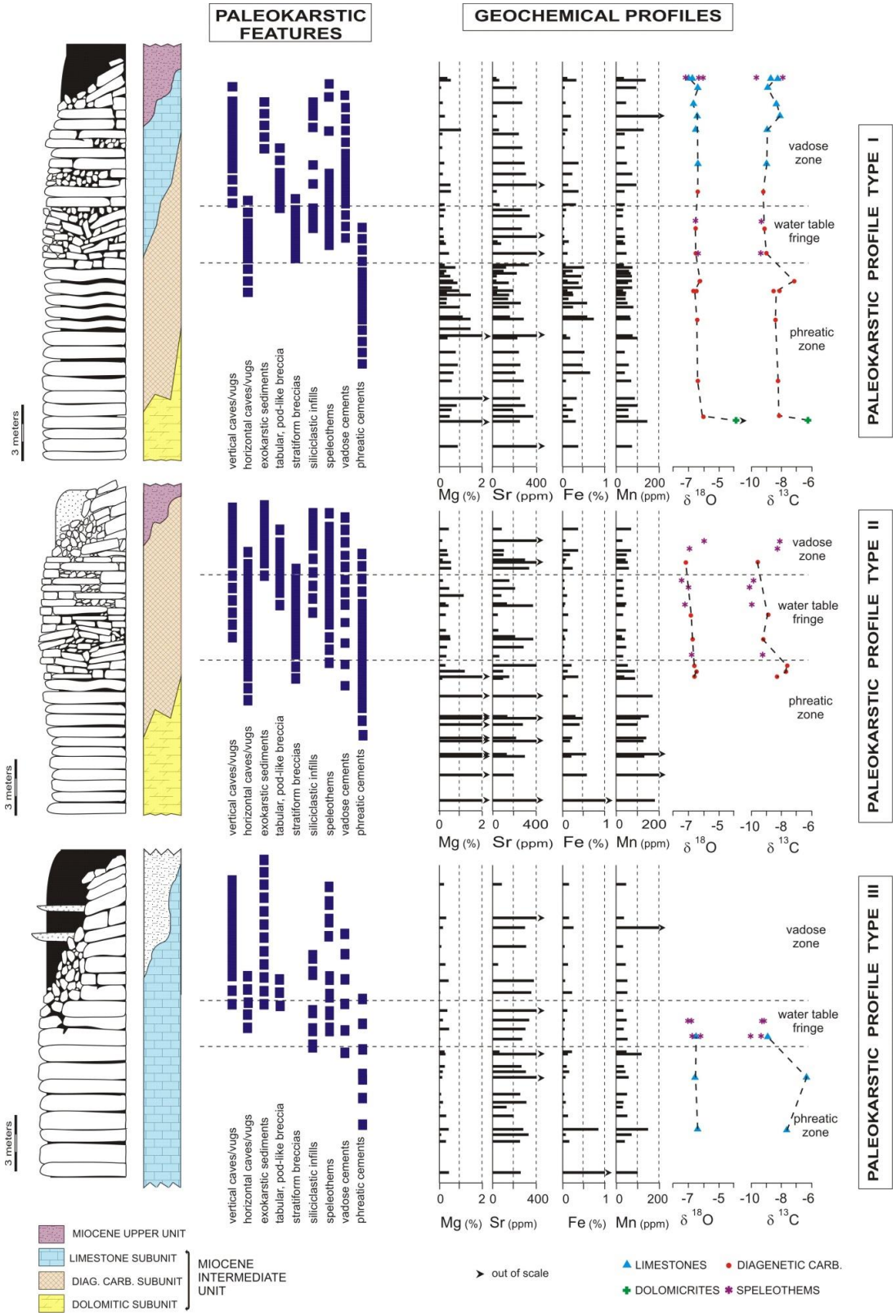

Figure 9. Environmental zonation of the top of the Miocene Intermediate Unit based on the integration of geological, petrographic, and geochemical (trace elements and stable isotopes) data for different parts of the study area (see Figure 8).

As the degree of closure or opening of the diagenetic system depends upon the water/rock ratio and the flow rate [41,56], the lowest Mg and Sr contents should be expected to correspond to carbonates lying in the water table fringe. In our case, this was true for magnesium, but for strontium, which is considered as a sensitive trace element reflecting the degree of closure of diagenetic systems under oxidizing conditions [41,57], an erratic trend was commonly observed throughout the profiles. This could be indicative of either water table fluctuations or the fact that Sr incorporation into diagenetic carbonates is also governed by other factors such as the composition of diagenetic fluids or biological (microbial) influences [5,41,58]. Regarding the latter point, biological influence on Sr incorporation into carbonate phases must not be ruled out since the influence of bioinduction in the growth of some diagenetic fabrics at the top of the Miocene Intermediate Unit has also been constrained [34,35].

The diagenetic carbonates and speleothems with the lowest Fe and Mn contents corresponded to those located in the water table fringe, that is, related to the highest flow rates. These elements most closely approach equilibrium with meteoric waters under oxidizing conditions, a typical situation where, as in the water table fringe, flow rates and consequently water-rock ratios are high [57]. This relationship is directly controlled by redox conditions (i.e., Eh increases as flow rates increase) and results in an inverse relation between the concentrations of Fe and Mn and the water-rock ratios.

The evolution of the stable isotope compositions within the speleothems reflects a lower variability of $\delta^{18}O$ with respect to $\delta^{13}C$, indicating that evaporation processes weakly influenced their formation [58,59]; however, we observed that some vadose speleothems were enriched in ^{18}O relative to their host-rock, indicating their formation was significantly influenced by evaporation. As observed in Figure 9, carbonates in the paleokarstic profiles showed an increase of $\delta^{13}C$ with depth, concurrent with constant $\delta^{18}O$ values, which well fits the model proposed [18]. This shift of the carbon isotopic signature takes place at shallow depth in the profiles, which provides evidence that the water table was near the surface [18,48,60].

4.4. Evolutionary Model of the Intra-Vallesian Paleokarst

Diagenetic facies (Diagenetic Carbonate Subunit), as here described, are characteristic products of meteoric diagenesis in near-surface environments [34,61–65], whose formation may be related to water table fluctuations [66] and/or major changes in basin paleogeography [35,62,67]. Additionally, several features demonstrate the subaerial and pre-burial nature of the Intra-Vallesian paleokarst such as (i) breccia deposits that include pseudospar and speleothem fragments, together with fluvial deposits capping the karst surface; and (ii) cave-fill deposits (clays, subarkoses and flowstones) within the subsurface karst system. By integrating morphological and petrological data, a hydrogeological or environmental zonation was established in the paleokarstic profiles defined at the top of the Miocene Intermediate Unit in different areas of the Madrid Basin. The vertical trends showed by both trace-element and stable isotope values throughout the profiles were used to complement the characterization and distribution of the diagenetic zones. Three main zones were differentiated: (i) the *paleo-vadose zone*, characterized by the development of exokarstic features such as vertically elongated caves and vugs, discontinuous banded and fibrous speleothems and pendant vadose cements, and the existence of tabular to podlike collapse breccia bodies in its lower part; (ii) the *paleo-water table fringe (paleo-epiphreatic zone)*, characterized by the wide development of stratiform endokarstic breccia bodies, the superimposition of both vadose and phreatic features, and the lowest Mg, Fe, and Mn contents in host-rock carbonates; and (iii) the *paleo-phreatic zone*; characterized by the dominance of isopachous phreatic cements, which is concomitant with a near absence of vadose features. In this case study, it is evident that Mg, Na, Sr, and $\delta^{18}O$ trends were not useful in establishing the hydrogeochemical zonation, though they are considered an aid for interpretation of the environmental conditions in which the karstification took place.

The carbonate and gypsiferous lacustrine sequences deposited during the Vallesian in the Madrid Basin were subject to early karstification. Under these conditions of meteoric diagenesis, both diagenetic stabilization of the mineral phases and karstification were genetically related in a rather short time

interval. The hydrogeological zonation of the paleokarst must be thus controlled by lithologies that show higher diagenetic potential, especially dolomite and gypsum. The dissolution of gypsum beds account mainly for the development of the karstic flow conduits.

Several authors [11,19,68] have interpreted the zones of phreatic diagenetic alteration to be representative of the dimensions of paleo-phreatic zones. Recent studies on the meteoric diagenesis of Holocene carbonate deposits indicate, however, that diagenetic alteration is mostly confined near the water table [12] and consequently, the distribution of the diagenetic carbonates is indicative of the fluctuation range of the water table. In our case study, some features provide evidence of the existence of this fluctuation throughout the paleokarstic profiles (Figure 9): (i) the erratic trends observed for some trace elements, especially Sr, through the profiles whichever area they developed; (ii) the common superimposition of phreatic and vadose cements both below and above the water table zone, which is especially clear in paleokarstic profiles of type II; and (iii) the great thickness and lateral extent of endokarstic features (breccia deposits, speleothems) across the profiles, which is also especially marked for profiles developed in the central part of the study area (type II).

The paleowater table fringe and the phreatic zone can be precisely fixed in karstic profiles of the northeastern area. However, in sections lying on the central and eastern parts of the basin, the water table fringe does not show as clear a pattern. This can be constrained by the specific lithologies (i.e., gypsum and limestone) that constitute the host-rock in these areas. Extensive dissolution of gypsum, which is widely distributed in central parts of the basin, would account for high relative oscillation of the water table within the paleokarst, leading to an apparent thicker water table fringe. In the eastern area, where the host-rock is mainly limestone, the diagenetic alteration is comparatively low and the hydrogeological zonation is less evidenced. In addition to these lithological constraints, other factors such as local tectonics [32,69,70] and the paleohydrological flow pattern in the basin at the time the paleokarst developed could also contribute to the variations in the distribution of karst features across the area.

The hydrological pattern deduced for the intra-Vallesian paleokarst [34] shows that in the northeastern and central areas, the recharge was mainly allogenic traversing marginal siliciclastic deposits, whereas in the eastern area, the allogenic recharge was more reduced and meteoric water reacted with the host carbonate, particularly limestones, before reaching the water table. Figure 10 shows the correlation among several paleokarstic profiles and provides a paleomorphological scheme for the intra-Vallesian paleokarst.

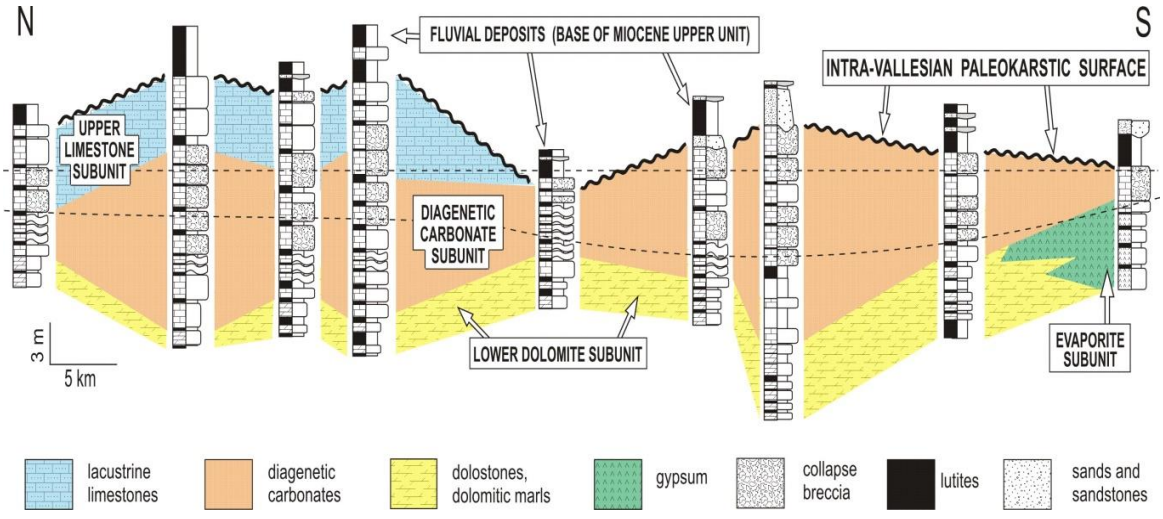

Figure 10. Environmental zonation of the top of the Miocene Intermediate Unit based on the integration of geological, petrographic, and geochemical data for different parts of the study area (see Figure 8).

As deduced from the correlation scheme, the paleogeography sketch of the region during the Vallesian show (Figure 11): (i) paleokarst profiles with thicker vadose zones and more stable water table fringes to the north, and (ii) profiles representing near surface and highly fluctuating water table fringe to the south.

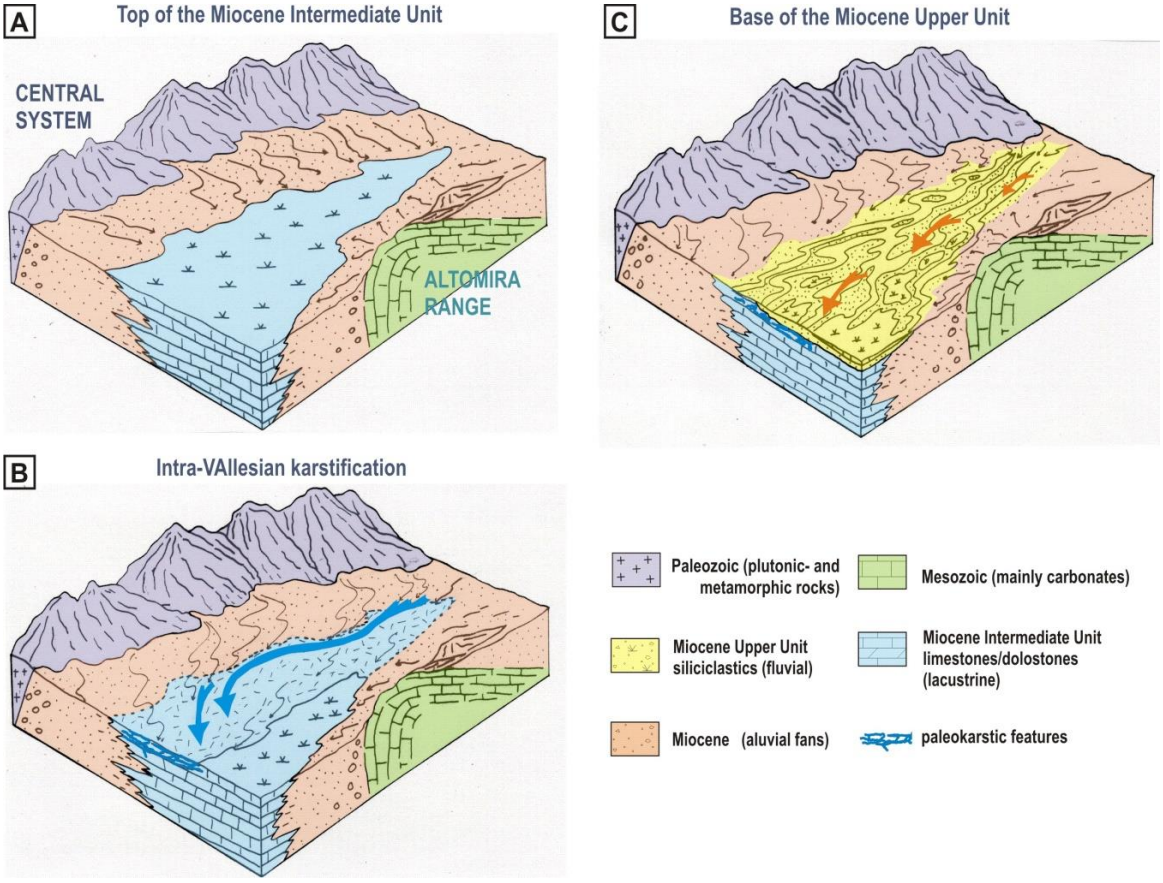

Figure 11. Late Miocene evolution and paleogeographical reconstruction (Madrid Basin). (**A**) Top of the Miocene Intermediate Unit: Generalized expansion of shallow lacustrine systems in a purely endorheic context. (**B**) Intra-Vallesian karstification: Relative uplift of materials of the Intermediate Unit with respect to the regional base level of the basin. Beginning of the change of the drainage system of the basin toward exorheic conditions. Generation of a low paleorelief with a N–S to NW–SE topographic gradient. Generation of endokarstic features, especially in the eastern areas of the central carbonate-evaporite facies. (**C**) Miocene Upper Unit: Sedimentation of exorheic fluvial siliciclastic facies (base of Upper Unit) on the intra-Vallesian exposure surface. Progressive loss of the paleokarst functionality. Progressive hierarchization of a fluvial network with a predominance of siliciclastic fluvial facies at the base and denoting an energy decrease toward the top of the unit (lacustrine facies) and toward the south of the basin.

The paleoaquifer system is envisaged as developed in a relatively shallow karst where the water table was near the surface. The paleotopography of the intra-Vallesian paleokarst surface may be estimated by analyzing the thickness of the sedimentary unit, which covers the paleokarst [71]. In the Madrid Basin, this is represented by the fluvio-lacustrine deposits of the Miocene Upper Unit, which correspond to the youngest endorheic deposits in the basin (Figure 11). Late Miocene–Pliocene alluvial fans were deposited over an erosion surface, representing the onset of the opening of the Madrid Basin to the Atlantic during the Plio-Quaternary, reflecting a clear deceleration of the tectonic deformation that resulted in uplift of the Central System and the Madrid Basin [33,72]. The thickness of the Miocene Upper Unit increased from 0–5 m in the north to 50–60 m to the south. Placing these values

together with the correlation scheme represented in Figure 10, a gradient from recharge to discharge zones throughout the karst could be deduced. In our case, this gradient is considered to have been lower than 2°, thus suggesting a very low relief of the Vallesian karstic surface. This endorheic–exorheic transition in the internal continental Madrid Basin highlights a major geodynamic change as is evidenced in other Iberian basins [62,67,73,74].

The obtained model could be applied to other regional cases where continental successions undergo short- to long-term meteoric diagenesis, especially if varied lithologies are present, which constrain fluctuations in the paleo-water table position. Other continental Tertiary basins in Spain and in other regions, show similar sedimentary-diagenetic evolution during Vallesian [75], that is, endorheic lacustrine systems including dolomite, gypsum, and limestone passing upward to diagenetically-complex carbonates and to fluvial siliciclastic-carbonate successions. Whichever the case, the reconstruction of paleokarstic profiles and subsequent paleogeographical interpretation must always be achieved by the integration of well-constrained regional, geomorphological, petrographic, and geochemical data.

5. Conclusions

An intra-Vallesian (Upper Miocene) paleokarst affecting the top of the Intermediate Miocene Unit in the continental intracratonic Madrid Basin (center Spain) was recognized. This paleokarst is a shallow, tabular-shaped karst that formed early after the deposition of the Miocene Intermediate Unit and shows a marked control by the depositional facies pattern and lithologies. This paleokarst represents an early pre-burial karst system developed on an unconfined carbonate-evaporite aquifer where the water movement was mainly gravity-controlled. By integrating morphological, petrological, and geochemical data, three hydrogeological or environmental zones were established throughout the paleokarstic profiles: (i) a paleo-vadose zone, characterized by vertically elongated caves and vugs, discontinuous banded and fibrous speleothems and pendant vadose cements, and the existence of tabular to podlike collapse breccia bodies in its lower part; (ii) a 3–7m thick paleo-epiphreatic zone (paleo-water table fringe), characterized by the wide development of bedding-parallel breccia bodies, the superimposition of both vadose and phreatic features, and the lowest Mg, Fe and Mn contents in host-rock carbonates; and (iii) a paleo-phreatic zone characterized by an increase in $\delta^{13}C$ values and the dominance of phreatic cementation, which is concomitant with the rare occurrence of vadose features.

The use of the paleo-water table fringe as a correlation level allows for a reconstruction of the paleogeography for the intra-Vallesian paleokarst. Accordingly, relative topographic highs to the north and topographic lows to the south draw the paleokarst landscape. This paleogeography is influenced by the larger occurrence of gypsum host-rocks, which caused the water table to be nearer to the surface and the oscillation fringe to be higher in the southern part of the basin. A paleogeographic reconstruction of the Madrid Basin during the late Vallesian was inferred from this analysis. Immediately overlaying the paleokarst surface are fluvio-lacustrine siliciclastic/carbonate facies belonging to the Miocene Upper Unit (Late Vallesian to Late Turolian). Their lowermost deposits consist of fluvial terrigenous facies deposited by approximately N–S fluvial streams, and pass upward into fluvio-lacustrine fresh-water limestones. The facies arrangement shown by the fluvial deposits is clearly different from that observed in the earlier Miocene units, and suggests a major paleogeographical change in the area during the Vallesian from endorheic to exorheic conditions. This intra-Vallesian paleokarst reflects a drastic paleoenvironmental and paleogeographic shift between the Intermediate and Superior Miocene units, which is related to a change from compressive to extensive conditions in the tectonic regime of the Madrid Basin. This tectonic event is correlated with other peripheral and interior basins in the Iberian Peninsula.

Author Contributions: Investigation, J.C.C., J.P.C., S.O., M.C.M.-C. and S.S.-M.; Writing–original draft, J.C.C., J.P.C., S.O., M.C.M.-C. and S.S.-M. All authors have read and agreed to the published version of the manuscript.

Funding: This study was supported with funding provided by Research Group VIGROB-095 of the University of Alicante and projects PB89-0032 and PB89-0047 of the Government of Spain.

Acknowledgments: We thank E. Rodríguez-Badiola and R. González (MNCN-CSIC) for their assistance during the geochemical and mineralogical analyses.

Conflicts of Interest: The authors declare no conflict of interest.

References

1. Wright, V.P. The recognition and interpretation of paleokarst: Two examples from the lower Carboniferous of South Wales. *J. Sediment. Petrol.* **1982**, *52*, 83–94.
2. Esteban, M.; Klappa, C.F. Subaerial exposure environment. In *Carbonate Depositional Environments*; Scholle, P.A., Bebout, D.G., Moore, C.H., Eds.; AAPG Memoir 33; AAPG: Tulsa, OK, USA, 1983; pp. 1–54.
3. Budd, D.A.; Gaswirth, S.B.; Oliver, W.L. Quantification of macroscopic subaerial exposure features in carbonate rocks. *J. Sediment. Petrol.* **2002**, *72*, 917–928. [CrossRef]
4. Railsback, B.L.; Holland, S.M.; Hunter, D.M.; Jordan, E.M.; Díaz, J.R.; Crowe, D.E. Controls on geochemical expression of subaerial exposure in Ordovician limestones from the Nashville Dome, Tennessee, U.S.A. *J. Sediment. Res.* **2003**, *73*, 790–805. [CrossRef]
5. Calner, M.; Lehnert, O.; Nõlvak, J. Palaeokarst evidence for widespread regression and subaerial exposure in the middle Katian (Upper Ordovician) of Baltoscandia: Significance for global climate. *Palaeogeogr. Palaeoclimat. Palaeoecol.* **2010**, *296*, 235–247. [CrossRef]
6. Pennos, C.; Lauritzen, S.E.; Vouvalidis, K.; Cowie, P.; Pechlivanidou, S.; Gkarlaouni, C.; Styllas, M.; Tsourlos, P.; Mouratidis, A. From subsurface to surface: A multidisciplinary approach to decoding uplift histories in tectonically-active karst landscapes. *Earth Surf. Process. Landf.* **2019**, *44*, 1710–1725. [CrossRef]
7. Jennings, J.N. *Karst Geomorphology*; Basil Blackwell Ltd.: New York, NY, USA, 1985.
8. Halley, R.B.; Harris, P.M. Freshwater cementation of a 1000 year-old oolite. *J. Sediment. Petrol.* **1979**, *49*, 969–988.
9. Strasser, A.; Davaud, E. Formation of Holocene limestone sequences by progradation, cementation, and erosion: Two examples from the Bahamas. *J. Sediment. Petrol.* **1986**, *56*, 422–428.
10. Budd, D.A. Petrographic products of freshwater diagenesis in Holocene ooid sands, Schooner Cays, Bahamas. *Carbonates Evaporites* **1988**, *3*, 143–163. [CrossRef]
11. Budd, D.A.; Vacher, H.L. Predicting the thickness of fresh-water lenses in carbonate paleo-islands. *J. Sediment. Petrol.* **1991**, *61*, 43–53.
12. McClain, M.E.; Swart, P.K.; Vacher, H.L. The hydrogeochemistry of early meteoric diagenesis in a Holocene deposit of biogenic carbonates. *J. Sediment. Petrol.* **1992**, *62*, 1008–1022.
13. Liu, N.; Wang, Z.; Li, X.; Liu, L.; Zhang, D.; You, L.; Luo, W.; Liu, X. Reef-carbonate diagenesis in the Pleistocene–Holocene of the well Xike#1, Xisha Islands, South China Sea: Implications on sea-level changes. *Carbonates Evaporites* **2019**, *34*, 1669–1687.
14. Land, L.S. Phreatic vs. vadose meteoric diagenesis of limestones: Evidence from a fossil water table. *Sedimentology* **1970**, *14*, 175–185. [CrossRef]
15. Steinen, R.P.; Matthews, R.K. Phreatic vs. vadose diagenesis: Stratigraphy and mineralogy of a cored bore hole on Barbados, W.I. *J. Sediment. Petrol.* **1973**, *43*, 1012–1020.
16. Pingitore, N.E. Vadose and phreatic diagenesis: Processes, products, and their recognition in coral reefs. *J. Sediment. Petrol.* **1976**, *46*, 985–1006.
17. Buchbinder, L.G.; Friedman, G.M. Vadose, phreatic, and marine diagenesis of Pleistocene-Holocene carbonates in a borehole: Mediterranean coast of Israel. *J. Sediment. Petrol.* **1980**, *50*, 953–962.
18. Allan, J.R.; Matthews, R.K. Isotope signatures associated with early meteoric diagenesis. *Sedimentology* **1982**, *29*, 709–817. [CrossRef]
19. Saller, A.H.; Moore, C.H. Meteoric diagenesis, marine diagenesis, and microporosity in Pleistocene and Oligocene limestones, Enewetak Atoll, Marshall, Islands. *Sediment. Geol.* **1989**, *63*, 253–272. [CrossRef]
20. Meyers, W.J. Carbonate cements: Their regional distribution and interpretation in Mississippian limestones of southwestern New Mexico. *Sedimentology* **1978**, *25*, 371–400. [CrossRef]
21. Moldovanyi, E.P.; Lohmann, K.C. Isotopic criteria for recognition of successive events of phreatic cementation, Sligo and Cupido Formations. *J. Sediment. Petrol.* **1984**, *54*, 972–985.

22. Beeunas, A.; Knauth, L.P. Preserved stable isotopic signature of subaerial diagenesis in the 1.2-b.y. Mescal Limestone, central Arizona: Implications for the timing and development of a terrestrial plant cover. *Geol. Soc. Am. Bull.* **1985**, *96*, 737–745. [CrossRef]
23. Given, R.K.; Lohmann, K.C. Isotopic evidence for the early meteoric diagenesis of the reef facies, Permian Reef Complex of West Texas and New Mexico. *J. Sediment. Petrol.* **1986**, *56*, 183–193.
24. Holail, H. Coordinated petrography-isotopic-chemical investigation of meteoric calcite cement (Jurassic-Pleistocene), Egypt. *Carbonates Evaporites* **1992**, *7*, 48–55. [CrossRef]
25. Li, Z.; Goldstein, R.H.; Franseen, E.K. Meteoric calcite cementation: Diagenetic response to relative fall in sea-level and effect on porosity and permeability, Las Negras area, southeastern Spain. *Sediment. Geol.* **2017**, *348*, 1–18. [CrossRef]
26. Craig, D.H. Caves and other features of Permian karst in San Andres dolomite, Yates Field reservoir, west Texas. In *Paleokarst*; James, N.P., Choquette, P.W., Eds.; Springer: New York, NY, USA, 1988; pp. 342–363.
27. Ford, D.C. Characteristics of dissolutional cave systems in carbonate rocks. In *Paleokarst*; James, N.P., Choquette, P.W., Eds.; Springer: New York, NY, USA, 1988; pp. 25–57.
28. Palmer, A.N. Stratigraphic and structural control of cave development and groundwater flow in the Mammoth Cave region. In *Karst hydrology: Concepts from the Mammoth Cave Area*; White, W.B., White, E.L., Eds.; Van Nostrand Reinhold: New York, NY, USA, 1989; pp. 293–316.
29. Calvo, J.P.; Alonso Zarza, A.M.; García del Cura, M.A. Models of Miocene marginal lacustrine sedimentation in response to varied depositional regimes and source areas in the Madrid basin (Central Spain). *Palaeogeogr. Palaeoclimat. Palaeoecol.* **1989**, *70*, 199–214. [CrossRef]
30. Calvo, J.P.; Hoyos, M.; Morales, J.; Ordóñez, S. Neogene stratigraphy, sedimentology and raw materials of the Madrid basin. *Paleontol. Evol.* **1990**, *2*, 63–95.
31. Cañaveras, J.C.; Calvo, J.P.; Hoyos, M.; Ordóñez, S. Palaeomorphologic features of an intra-Vallesian paleokarst, Tertiary Madrid basin. Significance of paleokarstic surfaces in continental basin analysis. In *Tertiary Iberian Basins*; Friend, P., Dabrio, C.J., Eds.; World and Regional Geology 6; Cambridge Univ. Press: Cambridge, UK, 1996; pp. 120–126.
32. Alonso-Zarza, A.M.; Calvo, J.P.; Silva, P.G.; Torres, T. Cuenca del Tajo. In *Geología de España*; Vera, J.A., Ed.; SGE-IGME: Madrid, Spain, 2004; pp. 556–561.
33. De Vicente, G.; Muñoz-Martín, A. The Madrid Basin and the Central System: A tectonostratigraphic analysis from 2D seismic lines. *Tectonophysics* **2013**, *602*, 259–285. [CrossRef]
34. Cañaveras, J.C.; Sánchez-Moral, S.; Calvo, J.P.; Hoyos, M.; Ordóñez, S. Dedolomites associated with karstification. An example of early dedolomitization in lacustrine sequences from the Tertiary Madrid Basin, central Spain. *Carbonates Evaporites* **1996**, *11*, 85–103. [CrossRef]
35. Rossi, C.; Cañaveras, J.C. Pseudospherulitic fibrous calcite in paleo-groundwater, unconformity-related diagenetic carbonates (Paleocene of the Áger basin and Miocene of the Madrid basin, Spain). *J. Sediment. Res.* **1999**, *69*, 224–238. [CrossRef]
36. Cerling, T.E.; Hay, R.L. An isotopic study of paleosol carbonates from Olduvai Gorge. *Quat. Res.* **1986**, *25*, 63–78. [CrossRef]
37. Andrews, J.E.; Riding, R.; Dennis, P.F. Stable isotopic composition of Recent freshwater cyanobacterial carbonates from the British Isles: Local and regional environmental controls. *Sedimentology* **1993**, *40*, 303–314. [CrossRef]
38. Theiling, B.P.; Railsback, L.B.; Holland, S.M.; Crowe, D.E. Heterogeneity in geochemical expression of subaerial exposure in limestones, and its implications for sampling to detect exposure surfaces. *J. Sediment. Res.* **2007**, *77*, 159–169. [CrossRef]
39. Baqués, V.; Travé, A.; Cantarero, I. Development of successive karstic systems within the Baix Penedès Fault zone (onshore of the Valencia Trough, NW Mediterranean). *Geofluids* **2014**, *14*, 75–94. [CrossRef]
40. Kahle, C.F. Surface and subsurface paleokarst, Silurian Lockport, and Pebbles Dolomites, Western Ohio. In *Paleokarst*; James, N.P., Choquette, P.W., Eds.; Springer: New York, NY, USA, 1988; pp. 58–80.
41. Barnaby, R.J.; Rimstidt, J.D. Redox conditions of calcite cementation interpreted from Mn and Fe contents of authigenic calcites. *Geol. Soc. Am. Bull.* **1989**, *101*, 795–804. [CrossRef]
42. Meyers, W.J. Carbonate cement stratigraphy of the Lake Valley Formation (Mississippian), Sacramento Mountains, New Mexico. *J. Sediment. Petrol.* **1974**, *44*, 837–861.

43. Bustillo, M.A.; Alonso-Zarza, A.M. Overlapping of pedogenesis and meteoric diagenesis in distal alluvial and shallow lacustrine deposits in the Madrid Miocene Basin, Spain. *Sediment. Geol.* **2008**, *198*, 255–271. [CrossRef]
44. Seibel, M.J.; James, N.P. Diagenesis of Miocene, incised valley-filling limestones; Provence, Southern France. *Sediment. Geol.* **2017**, *347*, 21–35. [CrossRef]
45. Gázquez, F.; Columbu, A.; De Waele, J.; Breitenbach, S.F.M.; Huangd, C.-R.; Shen, C.; Lu, Y.; Calaforra, J.M.; Mleneck-Vautraversa, M.J.; Hodell, D.A. Quantification of paleo-aquifer changes using clumped isotopes in subaqueous carbonate speleothems. *Chem. Geol.* **2018**, *493*, 246–257. [CrossRef]
46. Hendy, C.H. The isotopic geochemistry of speleothems-I. The calculation of the effects of different modes of formation on the isotopic composition of speleothems and their applicability as paleoclimatic indicators. *Geochim. Cosmochim. Acta* **1971**, *35*, 801–824. [CrossRef]
47. Veizer, J. Chemical diagenesis of carbonates: Theory and application of trace element techniques. In *Stable Isotopes in Sedimentary Geology*; SEPM Short Course no.10; SEPM: Tulsa, OK, USA, 1983; pp. 3–100.
48. Banner, J.L.; Hanson, G.N. Calculation of simultaneous isotopic and trace element variations during water-rock interaction with applications to carbonate diagenesis. *Geochim. Cosmochim. Acta* **1990**, *54*, 3123–3137. [CrossRef]
49. Banner, J.L. Application of the trace element and isotope geochemistry of strontium to studies of carbonate diagenesis. *Sedimentology* **1995**, *42*, 805–824. [CrossRef]
50. Kitano, Y.; Okumura, M.; Idogaki, M. Incorporation of sodium, chloride and sulfate with calcium carbonate. *Geochem. J.* **1975**, *84*, 75–84. [CrossRef]
51. Busemberg, E.; Plummer, L.N. Kinetic and thermodynamic factors controlling the distribution of SO_3^{2-} and Na^+ in calcites and selected aragonites. *Geochim. Cosmochim. Acta* **1985**, *49*, 713–725. [CrossRef]
52. White, A.F. Sodium coprecipitation in calcite and dolomite. *Chem. Geol.* **1978**, *23*, 65–72. [CrossRef]
53. Ishikawa, M.; Ichikumi, M. Uptake of sodium and potassium by calcite. *Chem. Geol.* **1978**, *42*, 137–146. [CrossRef]
54. Calvo, J.P.; Jones, B.F.; Bustillo, M.; Fort, R.; Alonso-Zarza, M.A.; Kendall, C. Sedimentology and geochemistry of carbonates from lacustrine sequences in the Madrid Basin, central Spain. *Chem. Geol.* **1995**, *123*, 173–191. [CrossRef]
55. Woo, K.S.; Anderson, T.F.; Sandberg, P.A. Diagenesis of skeletal and nonskeletal components of mid-Cretaceous limestones. *J. Sediment. Petrol.* **1993**, *63*, 18–32.
56. Lohmann, K.C. Geochemical patterns of meteoric diagenetic systems and their application to studies of paleokarst. In *Paleokarst*; James, N.P., Choquette, P.W., Eds.; Springer: New York, NY, USA, 1988; pp. 58–80.
57. Hudson, J.D. Stable isotopes and limestone lithification. *J. Geol. Soc. Lond.* **1977**, *133*, 637–660. [CrossRef]
58. Bellanca, A.; Calvo, J.P.; Censi, P.; Neri, R.; Pozo, M. Recognition of lake-level changes in Miocene lacustrine units, Madrid basin, Spain—Evidences from facies analysis, isotope geochemistry and clay mineralogy. *Sediment. Geol.* **1992**, *76*, 135–153. [CrossRef]
59. Fantidis, J.; Ehhalt, D.H. Variations of the carbon and oxygen isotopic composition in stalagmites and stalactites: Evidence of non-equilibrium isotopic fractionation. *Earth Planet. Sci. Lett.* **1970**, *10*, 136–144. [CrossRef]
60. Videtich, P.E.; Matthews, R.K. Origin of discontinuity surfaces in limestones: Isotopic and petrographic data, Pleistocene of Barbados, West Indies. *J. Sediment. Petrol.* **1980**, *50*, 971–980.
61. Lee, M.R.; Harwood, G.M. Dolomite calcitization and cement zonation related to uplift of the Raisby Formation (Zechstein carbonate), northeast England. *Sediment. Geol.* **1989**, *65*, 285–305. [CrossRef]
62. Arenas, C.; Alonso Zarza, A.M.; Pardo, G. Dedolomitization and other diagenetic processes in Miocene lacustrine deposits, Ebro Basin (Spain). *Sediment. Geol.* **1999**, *125*, 23–45. [CrossRef]
63. Nader, F.H.; Swennen, R.; Keppens, E. Calcitization/dedolomitisation of Jurassic dolostones (Lebanon): Results from petrographic and sequential geochemical analyses. *Sedimentology* **2008**, *55*, 1467–1485. [CrossRef]
64. Hauck, T.E.; Corlett, H.J.; Grobe, M.; Walton, E.L.; Sansjofre, P. Meteoric diagenesis and dedolomite fabrics in precursor primary dolomicrite in a mixed carbonate–evaporite system. *Sedimentology* **2018**, *65*, 1827–1858. [CrossRef]
65. Schoenherr, J.; Reuning, L.; Hallenberger, M.; Lüders, V.; Lemmens, L.; Biehl, B.C.; Lewin, A.; Leupold, M.; Wimmers, K.; Strohmenger, C.J. Dedolomitization: Review and case study of uncommon mesogenetic formation conditions. *Earth-Sci. Rev.* **2018**, *185*, 780–805. [CrossRef]

66. Colson, J.; Cojan, I. Groundwater dolocretes in a lake-marginal environment: An alternative model for dolocrete formation in continental settings (Danian of the Provence Basin, France). *Sedimentology* **1996**, *43*, 175–188. [CrossRef]
67. Armenteros, I. Contribución al conocimiento del Mioceno lacustre de la Cuenca del Duero (sector centro-oriental, Valladolid-Peñafiel-Sacramenia-Cuéllar). *Acta Geol. Hisp.* **1991**, *2*, 97–131.
68. Wagner, P.D.; Matthews, R.K. Porosity preservation in the Upper Smackover (Jurassic) Carbonate Grainstone, WalkerCreek field, Arkansas: Response of paleophreatic lenses to burial processes. *J. Sediment. Petrol.* **1982**, *52*, 3–18. [CrossRef]
69. Rodríguez-Aranda, J.P.; Muñoz, A.; Giner, J.L.; Cañaveras, J.C. Estructuras tectónicas en el basamento de la Cuenca de Madrid y su reflejo en la cobertera sedimentaria. *Geogaceta* **1995**, *18*, 19–22.
70. Hoyos, M.; Doblas, M.; Sánchez-Moral, S.; Cañaveras, J.C.; Ordóñez, S.; Sesé, C.; Sanz-Rubio, E.; Mahecha, V. Hydration diapirism: A climate-related initiation of evaporite mounds in two continental Neogene basins of central Spain. In *Salt Tectonics*; Alsop, G.I., Blundell, D.J., Davison, I., Eds.; Geological Society Special Publication: London, UK, 1996; Volume 100, pp. 49–63.
71. Sando, W.J. Madison Limestone (Mississippian) paleokarst: A geologic synthesis. In *Paleokarst*; James, N.P., Choquette, P.W., Eds.; Springer: New York, NY, USA, 1988; pp. 256–277.
72. Karampaglidis, T.; Benito-Calvo, A.; Rodés, A.; Braucherd, R.; Pérez-González, A.; Pares, J.; Stuart, F.; Di Nicola, L.; Bourlesd, D. Pliocene endorheic-exhoreic drainage transition of the Cenozoic Madrid Basin (Central Spain). *Glob. Planet. Chang.* **2020**, *194*, 103295. [CrossRef]
73. Stokes, M.; Mather, A.E. Tectonic origin and evolution of a transverse drainage: The Rio Almazora. In: Betic Cordillera, southeast Spain. *Geomorphology* **2003**, *50*, 59–81. [CrossRef]
74. Cunha, P.P. Cenozoic basins of Western Iberia: Mondego, lower Tejo and Alvalade basins. In *The Geology of Iberia: A Geodynamic Approach*; Regional Geology Reviews; Quesada, C., Oliveira, J.T., Eds.; Springer International Publishing: Cham, Switzerland, 2019; pp. 105–130.
75. Calvo, J.P.; Damms, R.; Morales, J.; López-Martínez, N.; Agustí, J.; Anadón, P.; Armenteros, I.; Cabrera, L.; Civis, J.; Corrochano, A.; et al. Up-to-date Spanish continental Neogene synthesis and paleoclimatic interpretation. *Rev. Soc. Geol. Esp.* **1993**, *6*, 19–40.